Communications on Applied Mathematics and Computation (2019) 1:117–139
https://doi.org/10.1007/s42967-019-0007-x

ORIGINAL PAPER

Multiscale Radiative Transfer in Cylindrical Coordinates

Wenjun Sun[1] · Song Jiang[1] · Kun Xu[2]

Received: 19 June 2018 / Revised: 24 September 2018 / Accepted: 27 September 2018 /
Published online: 12 March 2019

Abstract
The radiative transfer equations in cylindrical coordinates are important in the application of inertial confinement fusion. In comparison with the equations in Cartesian coordinates, an additional angular derivative term appears in the cylindrical case. This term adds great difficulty for a numerical scheme to keep the conservation of total energy. In this paper, based on weighting factors, the angular derivative term is properly discretized, and the interface fluxes in the radial r-direction depend on such a discretization as well. A unified gas kinetic scheme (UGKS) with asymptotic preserving property for the gray radiative transfer equations is constructed in cylindrical coordinates. The current UGKS can naturally capture the radiation diffusion solution in the optically thick regime with the cell size being much larger than photon's mean free path. At the same time, the current UGKS can present accurate solutions in the optically thin regime as well. Moreover, it is a finite volume method with total energy conservation. Due to the scale-dependent time evolution solution for the interface flux evaluation, the scheme can cover multiscale transport mechanism seamlessly. The cylindrical hohlraum tests in inertial confinement fusion are used to validate the current approach, and the solutions are compared with implicit Monte Carlo result.

Keywords Cylindrical coordinate system · Gray radiative equations · Multiscale transport · Unified gas kinetic scheme

Mathematics Subject Classification 85A25 · 82C80 · 82C70 · 82C40

✉ Song Jiang
jiang@iapcm.ac.cn

Wenjun Sun
sun_wenjun@iapcm.ac.cn

Kun Xu
makxu@ust.hk

[1] Institute of Applied Physics and Computational Mathematics, P.O. Box 8009, Beijing 100088, China

[2] Department of Mathematics, Hong Kong University of Science and Technology, Clear Water Bay, Kowloon, Hong Kong, China

1 Introduction

In this paper, we continue our study of developing asymptotic preserving schemes for various radiative transfer systems. The current research is to propose an asymptotic preserving scheme for the gray radiative transfer equations in the cylindrical coordinate system. The radiation transport in such a geometry is important in laser-driven inertial confinement fusion (ICF), such as in the study of the popular hohlraum problem. Different from radiative transport equations in Cartesian coordinates, an additional angular derivative appears in the cylindrical case. This brings great difficulty to construct a numerical scheme with total energy conservation and capture transport physics in optically thin and optically thick regions uniformly.

The system of the gray radiative transfer equations models the radiation energy transport and exchange with background material. It is a simplification of the full transporting equations, but keeps the key ingredients in the transport process. For radiation, the background material properties influence greatly on the way of energy transport. For a low opacity (background) material, the interaction between the radiation and material is weak, and the radiation propagates in a transparent way. The numerical method in this regime is well defined by tracking the rays through upwind discretization of the streaming term in the equations, such as the step method. However, for a high opacity (background) material, there is severe interaction between radiation and material with a diminishing photon's mean free path. As a result, the radiation propagates as a diffusive process. To solve the radiative transfer equation, the spatial mesh size is usually required to be comparable to the photon's mean free path, which is very small in the optically thick (i.e., high opacity) regime. This kind of approach for solving kinetic equations is associated with huge computational cost. Instead, the macroscopic diffusion equation is usually solved in the optically thick region to get the solution efficiently. But, the diffusion equation is not accurate in the optically thin (i.e., low opacity) region, and the boundary between optically thin and thick regions is difficult to be clearly defined. To accurately present the physical transport process efficiently, a multiscale method has to be developed. This method should be able to connect solutions in the optically thin and thick regions seamlessly. Intensive investigation has been devoted on the development of such a multiscale method in the past decades, i.e., the search for the so-called asymptotic preserving (AP) methods [6–10, 12].

Recently, unified gas kinetic schemes (UGKS) with AP properties have been proposed for linear radiation transport model [17], gray radiative transfer equations [19, 21], and frequency-dependent radiative transfer equations [20, 22, 23]. All these schemes are designed in a Cartesian coordinate system. The success of the UGKS is mainly from the coupled treatment of particle transport and collision in the flux evaluation in a finite volume scheme [25]. This time and scale evolving solution at a cell interface covers the transport physics from the kinetic particle free transport to the macroscopic diffusion limit with the variation of the ratio of the time step $t \in [t^n, t^{n+1}]$ over the particle collision time τ. The local ratio $\Delta t/\tau$, controls different photon's transport behavior in the optically thin region $\Delta t < \tau$ and optically thick region $\Delta t \ll \tau$. As a result, the solutions in different regimes can be obtained simultaneously due to the local variation of $\Delta t/\tau$. In UGKS, the cell size and time step used are not limited by the particle mean free path and collision time [2, 5].

In many engineering applications, e.g., in ICF, the use of cylindrical coordinates is much convenient to solve the physical problems. In this paper, for the first time, a unified gas kinetic scheme will be developed for the radiative transfer equations in the cylindrical coordinate [18]. The developed scheme is asymptotic preserving for the gray radiative transfer equations in *RZ*

cylindrical coordinates, where the diffusive solution will be captured accurately in the optically thick region without using a cell size being smaller than photon's mean free path. Besides the diffusion limit, the scheme can also capture the solution in the optically thin regime. For the current finite volume scheme, the total energy, i.e., the sum of radiation and material thermal ones in the system, will be conserved precisely. A cylindrical hohlraum example in ICF will be studied by the current scheme.

This paper is organized as follows. Section 2 gives the model equations of gray radiation transfer in the cylindrical *RZ* geometry. Section 3 presents the unified gas kinetic scheme in such a coordinate system. Section 4 gives the asymptotic preserving analysis for the cylindrical gray radiative transfer equations. In Sect. 5, numerical cylindrical hohlraum problems in inertial confinement fusion are included to demonstrate the accuracy and robustness of the proposed scheme. The conclusion is given in Sect. 6.

2 Gray Radiative Transfer Equations in Cylindrical *RZ* Geometry

The gray radiative transfer equations model the radiative transfer and energy exchange between radiation and material. In the cylindrical *RZ* geometry, the scaled equations can be written in the following form:

$$\begin{cases} \dfrac{\epsilon}{c}\dfrac{\partial I}{\partial t} + \dfrac{\mu}{r}\dfrac{\partial (rI)}{\partial r} + \xi\dfrac{\partial I}{\partial z} - \dfrac{1}{r}\dfrac{\partial(\eta I)}{\partial \vartheta} = \dfrac{\sigma}{\epsilon}\Big(\dfrac{1}{4\pi}acT^4 - I\Big), \\ \epsilon^2 C_v \dfrac{\partial T}{\partial t} \equiv \epsilon^2 \dfrac{\partial U}{\partial t} = \sigma\Big(\displaystyle\int I \mathrm{d}\vec{\Omega} - acT^4\Big). \end{cases} \tag{2.1}$$

The cylindrical coordinate system is given in Fig. 1, where $\xi = \cos\theta$, $\mu = \sin\theta\cos\vartheta$, and $\eta = \sin\theta\sin\vartheta$. Here, the spatial variable is denoted by $\vec{x} = (z, r)$, $\vec{\Omega} = (\xi, \mu, \eta)$ is the angular variable, and t is the time variable, $I(\vec{x}, \vec{\Omega}, t)$ is the radiation intensity, $T(\vec{x}, t)$ is the material temperature, $\sigma(\vec{x}, T)$ is the opacity, a is the radiation constant, c is the speed of light, $\epsilon > 0$ is the Knudsen number, and $U(\vec{x}, t)$ is the material energy density. For the simplicity of presentation, we have omitted the internal source and scattering terms in (2.1).

For the small parameter ϵ, Eq. (2.1) is a relaxation model for the radiation intensity to the local thermodynamic equilibrium, in which the emission source is a Planckian at the local material temperature:

$$\frac{1}{4\pi}\sigma acT^4.$$

The material temperature $T(\vec{x}, t)$ and the material energy density $U(\vec{x}, t)$ are related by

$$\frac{\partial U}{\partial T} = C_v > 0,$$

where $C_v(\vec{x}, t)$ is the heat capacity.

At the small parameter limit $\epsilon \to 0$, Larsen et al. [11] have shown that, away from boundaries and initial times, the intensity I approaches to a Planckian at the local temperature, i.e.,

$$I^{(0)} = \frac{1}{4\pi}ac(T^{(0)})^4,$$

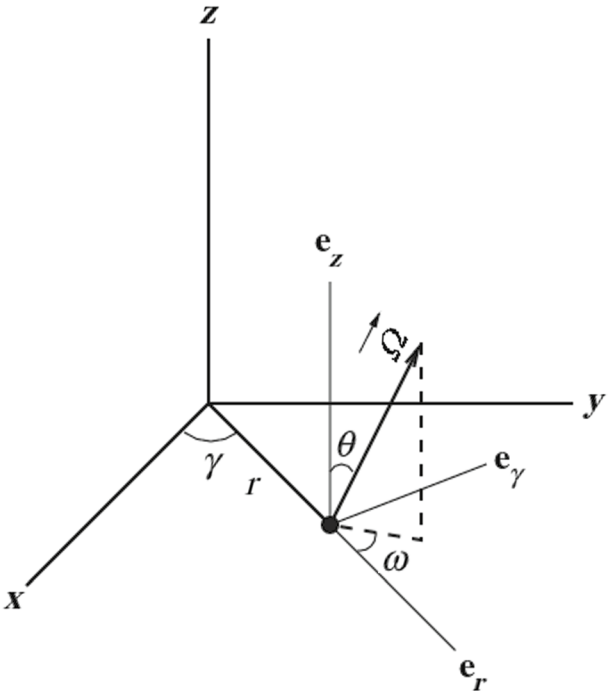

Fig. 1 Coordinate system for *RZ* geometry

and the corresponding local temperature $T^{(0)}$ satisfies the following nonlinear diffusion equation:

$$\frac{\partial}{\partial t}U(T^{(0)}) + a\frac{\partial}{\partial t}(T^{(0)})^4 = \frac{1}{r}\frac{\partial}{\partial r}\left(\frac{rac}{3\sigma}\frac{\partial (T^{(0)})^4}{\partial r}\right) + \frac{\partial}{\partial z}\left(\frac{ac}{3\sigma}\frac{\partial (T^{(0)})^4}{\partial z}\right). \tag{2.2}$$

In this paper, we shall construct an AP scheme for (2.1) in cylindrical coordinates. A discrete ordinate method will be constructed to solve the radiative transfer equation (2.1). The scheme has asymptotic preserving (AP) property for the gray radiation transfer equations (2.1), thus leading to a correct discretization of the diffusion limit equation (2.2) when ϵ is small. At the same time, the scheme is uniformly stable in ϵ.

3 Unified Gas Kinetic Scheme for System (2.1)

All previous unified gas kinetic schemes for radiative transfer equations are constructed in Cartesian coordinates [19–21]. In cylindrical coordinates, a proper discretization of angular derivative in the radiative system (2.1) is very important for the implementation of total energy conservation. The method in [18] for the discretization of angular derivative will be used in the current UGKS. In the following, we present the UGKS

for solving the system (2.1) numerically. We first discretize the first radiative transfer equation in the system (2.1); then solve the material energy equation in Sect. 3.4.

3.1 Angular Discretization

For the angular discretization, it is standard to use a symmetric quadrature set with N levels of discrete ξ values, and at each nth level there are M_n number of discrete μ values, see [13] for details. Certainly, other quadrature sets are also available. Our scheme can use other quadrature set which is symmetric and has weights summing to 4π. For a symmetrical RZ coordinate system, only the case of $\eta > 0$ is considered. For the discrete ordinate discretization in this paper, the angular flux is evaluated at every (m, n) discrete direction in the quadrature set, with directions $\vec{\Omega}_{m,n} = (\xi_{m,n}, \mu_{m,n}, \eta_{m,n})$ and integration weight $\omega_{m,n}$.

With the definition $\phi = acT^4$ and angular discretization, the radiative transfer equation of system (2.1) in the discrete ordinate discretization becomes

$$\begin{cases} \dfrac{\epsilon}{c}\dfrac{\partial I_{m,n}}{\partial t} + \dfrac{\mu_{m,n}}{r}\dfrac{\partial (rI_{m,n})}{\partial r} + \xi_{m,n}\dfrac{\partial I_{m,n}}{\partial z} \\ + \dfrac{\alpha_{m+\frac{1}{2},n} I_{m+\frac{1}{2},n} - \alpha_{m-\frac{1}{2},n} I_{m-\frac{1}{2},n}}{r\omega_{m,n}} = \dfrac{\sigma}{\epsilon}\left(\dfrac{1}{2\pi}\phi - I_{m,n}\right), \\ \alpha_{m+\frac{1}{2},n} = \alpha_{m-\frac{1}{2},n} - \mu_{m,n}\omega_{m,n}, \\ \alpha_{\frac{1}{2},n} = \alpha_{M_n+\frac{1}{2},n} = 0. \end{cases} \tag{3.1}$$

Given the definitions in Eq. (3.1), it is easy to show that these α-s preserve a constant solution [18]. For a constant solution with zero gradient, the solution should satisfy

$$\frac{\mu_{m,n} I_{m,n}}{r} + \frac{\alpha_{m+\frac{1}{2},n} I_{m+\frac{1}{2},n} - \alpha_{m-\frac{1}{2},n} I_{m-\frac{1}{2},n}}{r\omega_{m,n}} = 0,$$

which imposes a constraint on α in Eq. (3.1). With angular derivative differences in Eq. (3.1), $I_{m,n}$ and $I_{m+\frac{1}{2},n}$ are connected. To determine the solution, we solve $\mu = -\sqrt{1-\xi^2}$ for the starting direction angular flux on each ξ-level to obtain $I_{1/2,n}$ at angular position $\vartheta = \pi$. The resulting transport equation in the starting direction is equivalent to a transport equation in XY geometry along the starting direction of $\vec{\Omega}_{1/2,n} = (\xi_n, -\sqrt{1-\xi_n^2}, 0)$, which is given by

$$\frac{\epsilon}{c}\frac{\partial I_{1/2,n}}{\partial t} + \mu_{1/2,n}\frac{\partial (I_{1/2,n})}{\partial r} + \xi_{1/2,n}\frac{\partial I_{1/2,n}}{\partial z} = \frac{\sigma}{\epsilon}\left(\frac{1}{2\pi}\phi - I_{1/2,n}\right). \tag{3.2}$$

Up to now, we still need to construct one more relationship between $I_{m,n}$ and $I_{m+1/2,n}$ to close the system. A weighted diamond relationship between angular fluxes at the discrete ordinate points and the points between them [18] is used. This relationship is given by

$$I_{m,n} = \tau_{m,n} I_{m+\frac{1}{2},n} + (1-\tau_{m,n}) I_{m-\frac{1}{2},n}, \tag{3.3}$$

where the values of $\tau_{m,n}$ are defined such that a linear solution in μ will be preserved, i.e.,

$$\mu_{m,n} = \tau_{m,n}\mu_{m+\frac{1}{2},n} + (1-\tau_{m,n})\mu_{m-\frac{1}{2},n}, \tag{3.4}$$

with

$$\begin{cases} \mu_{m+\frac{1}{2},n} = \sqrt{1-\xi_n^2}\cos(\vartheta_{m+\frac{1}{2},n}), \\ \vartheta_{m+\frac{1}{2},n} = \vartheta_{m-\frac{1}{2},n} - \dfrac{\pi\omega_{m,n}}{\sum_{m=1}^{m=M_n}\omega_{m,n}}, \\ \vartheta_{\frac{1}{2},n} = \pi. \end{cases} \tag{3.5}$$

By virtue of the relation (3.3), the first equation in (3.1) for non-staring direction point can be rewritten as

$$\begin{aligned} &\frac{\epsilon}{c}\frac{\partial I_{m,n}}{\partial t} + \frac{\mu_{m,n}}{r}\frac{\partial(rI_{m,n})}{\partial r} + \xi_{m,n}\frac{\partial I_{m,n}}{\partial z} \\ &+\frac{\frac{\alpha_{m+1/2,n}}{\tau_{m,n}}I_{m,n} - \left(\frac{1-\tau_{m,n}}{\tau_{m,n}}\alpha_{m+1/2,n} + \alpha_{m-1/2,n}\right)I_{m-1/2,n}}{r\omega_{m,n}} = \frac{\sigma}{\epsilon}\left(\frac{1}{2\pi}\phi - I_{m,n}\right). \end{aligned} \tag{3.6}$$

This completes the angular discretization for Eq. $(2.1)_1$ at the starting direction point (3.2) and other points (3.6).

3.2 Time and Spatial Discretizations

Let $z_i = i\Delta z$, $r_j = j\Delta r$ and $t^k = k\Delta t$ $(i,j,k \in \mathbb{Z})$ be the uniform mesh in Cartesian coordinates, where these Δz, Δr and Δt are the mesh sizes in the z-, r- and t-directions, respectively; and let $C_{i,j}$ denote the cell $\{(z,r):\ z_{i-1/2} < z < z_{i+1/2}, r_{j-1/2} < r < r_{j+1/2}\}$, where $z_{i-1/2} = (i-\frac{1}{2})\Delta z$ and $r_{j-1/2} = (j-\frac{1}{2})\Delta r$ are the cell interfaces.

Let $I^k_{i,j,m,n} = \frac{\int_{C_{i,j}} I_{m,n}(z,r,t^k)r\mathrm{d}z\mathrm{d}r}{\int_{C_{i,j}} r\mathrm{d}z\mathrm{d}r}$ denote the cell averaged value of the variable $I_{m,n}$ at time t^k over cell (i,j) with cell mass center $(z_{i,j}, r_{i,j})$ calculated by

$$z_{i,j} = \frac{\int_{C_{i,j}} zr\mathrm{d}z\mathrm{d}r}{\int_{C_{i,j}} r\mathrm{d}z\mathrm{d}r}, \quad r_{i,j} = \frac{\int_{C_{i,j}} r^2\mathrm{d}z\mathrm{d}r}{\int_{C_{i,j}} r\mathrm{d}z\mathrm{d}r}. \tag{3.7}$$

Since the starting direction equation (3.2) is similar to the one in Cartesian coordinates, the aforementioned method in Cartesian coordinates (see [19–21]) can be used directly to discretize (3.2); hence, we omit the details of discretization here. For the non-starting direction $\Omega_{m,n}$, we integrate Eq.(3.6) over the cell (i,j) from time t^k to $t^k + \Delta t$ to give a conservative finite volume numerical scheme for Eq.(3.6) in the following form:

$$
\begin{aligned}
I_{i,j,m,n}^{k+1} = & I_{i,j,m,n}^{k} + \frac{\Delta t}{V_{i,j}}(F_{i-1/2,j,m,n} - F_{i+1/2,j,m,n}) \\
& + \frac{\Delta t}{V_{i,j}}(H_{i,j-1/2,m,n} - H_{i,j+1/2,m,n}) \\
& - \frac{c\Delta t}{\epsilon} \frac{\frac{\alpha_{m+1/2,n}}{\tau_{m,n}} I_{i,j,m,n}^{k+1} - \left(\frac{1-\tau_{m,n}}{\tau_{m,n}}\alpha_{m+1/2,n} + \alpha_{m-1/2,n}\right) I_{i,j,m-1/2,n}^{k+1}}{V_{i,j}\omega_{m,n}/A_{i,j}} \\
& + c\Delta t \left\{ \frac{\sigma}{\epsilon^2}\left(\frac{1}{2\pi}\tilde{\phi}_{i,j} - \tilde{I}_{i,j,m,n}\right)\right\}.
\end{aligned}
\tag{3.8}
$$

Here, $F_{i\pm1/2,j,m,n}$ and $H_{i,j\pm1/2,m,n}$ are the time-dependent numerical fluxes in the z- and r-directions across the cell interfaces, respectively, $V_{i,j} = \int_{C_{i,j}} r\mathrm{d}z\mathrm{d}r$ is the cell volume, and $A_{i,j} = \int_{C_{i,j}} \mathrm{d}z\mathrm{d}r$ is the area. The specific formulations for some terms on the right-hand side of (3.8) are given by

$$
\begin{aligned}
F_{i-1/2,j,m,n} =& \frac{c}{\epsilon\Delta t}\int_{t^k}^{t^{k+1}} \int_{E_{i-\frac{1}{2},j}} \xi_{m,n} r I_{m,n}(t, z, r, \mu_{m,n}, \xi_{m,n})\mathrm{d}S\mathrm{d}t \\
\simeq& \frac{cS_{i-\frac{1}{2},j}\xi_{m,n}}{\epsilon\Delta t}\int_{t^k}^{t^{k+1}} I_{m,n}(t, z_{i-\frac{1}{2}}, r_j, \mu_{m,n}, \xi_{m,n})\mathrm{d}t, \\
F_{i+1/2,j,m,n} =& \frac{c}{\epsilon\Delta t}\int_{t^k}^{t^{k+1}} \int_{E_{i+\frac{1}{2},j}} \xi_{m,n} r I_{m,n}(t, z, r, \mu_{m,n}, \xi_{m,n})\mathrm{d}S\mathrm{d}t \\
\simeq& \frac{cS_{i+\frac{1}{2},j}\xi_{m,n}}{\epsilon\Delta t}\int_{t^k}^{t^{k+1}} I_{m,n}(t, z_{i+\frac{1}{2}}, r_j, \mu_{m,n}, \xi_{m,n})\mathrm{d}t, \\
H_{i,j-1/2,m,n} =& \frac{c}{\epsilon\Delta t}\int_{t^k}^{t^{k+1}} \int_{E_{i,j-\frac{1}{2}}} \mu_{m,n} r I_{m,n}(t, z, r, \mu_{m,n}, \xi_{m,n})\mathrm{d}S\mathrm{d}t \\
\simeq& \frac{c\mu_{m,n}\Delta z}{\epsilon\Delta t}\int_{t^k}^{t^{k+1}} r_{i,j-\frac{1}{2}} I_{m,n}(t, z_i, r_{j-\frac{1}{2}}, \mu_{m,n}, \xi_{m,n})\mathrm{d}t, \\
H_{i,j+1/2,m,n} =& \frac{c}{\epsilon\Delta t}\int_{t^k}^{t^{k+1}} \int_{E_{i,j+\frac{1}{2}}} \mu_{m,n} r I_{m,n}(t, z, r, \mu_{m,n}, \xi_{m,n})\mathrm{d}S\mathrm{d}t \\
\simeq& \frac{c\mu_{m,n}\Delta z}{\epsilon\Delta t}\int_{t^k}^{t^{k+1}} r_{i,j+\frac{1}{2}} I_{m,n}(t, z_i, r_{j+\frac{1}{2}}, \mu_{m,n}, \xi_{m,n})\mathrm{d}t, \\
\tilde{\phi}_{i,j} =& \frac{1}{\Delta t V_{i,j}}\int_{t^k}^{t^{k+1}} \int_{C_{i,j}} r\phi(t, z, r)\mathrm{d}z\mathrm{d}r\mathrm{d}t, \\
\tilde{I}_{i,j,m,n} =& \frac{1}{V_{i,j}\Delta t}\int_{t^k}^{t^{k+1}} \int_{C_{i,j}} r I_{m,n}(t, z, r, \mu_{m,n}, \xi_{m,n})\mathrm{d}z\mathrm{d}r\mathrm{d}t,
\end{aligned}
\tag{3.9}
$$

where the notations $E_{i\pm\frac{1}{2},j}, E_{i,j\pm\frac{1}{2}}$ refer to the edges of the cell $C_{i,j}$, and $S_{i\pm\frac{1}{2},j}, S_{i,j\pm\frac{1}{2}}$ are the corresponding rotation areas of the edges.

To update the system (3.8), we have to determine all terms in (3.9) explicitly. First, it is easy to see that the term $\tilde{I}_{i,j,m,n}$ in (3.9) can be approximated implicitly by

$$\tilde{I}_{i,j,m,n} \approx I^{k+1}_{i,j,m,n},$$

which should be combined with the same term on the left-hand side of Eq. (3.8).

The angular boundary function $I^{k+1}_{i,j,m-1/2,n}$ in (3.8) is given by solving the starting direction equation (3.2) to obtain $I^{k+1}_{i,j,1/2,n}$ first, then goes to the relation (3.3). The formula for $\tilde{\phi}_{i,j}$ in (3.9) will be determined later. In the following, we present the construction for the interface fluxes $F_{i\pm1/2,j,m,n}$ and $H_{i,j\pm1/2,m,n}$ in (3.9).

3.3 Construction of the Interface Fluxes in (3.9)

For the *RZ* cylindrical coordinate system, the interface fluxes $F_{i\pm1/2,j,m,n}$ in the z-direction can be constructed in the same way as the case in the Cartesian coordinate system. In cylindrical case, we only need to get the expression for the interface fluxes $H_{i,j\pm1/2,m,n}$ in the r-direction in Eq. (3.8), which is a generalization of the method in [17, 25]. For the r-direction flux $H_{i,j-1/2,m,n}$ close to the singular point $r = 0$, the following initial value problem at the cell interface $z = z_i, r = r_{j-1/2}$ is solved,

$$\begin{cases} \dfrac{\epsilon}{c}\dfrac{\partial(rI_{m,n})}{\partial t} + \mu_{m,n}\dfrac{\partial(rI_{m,n})}{\partial r} + \dfrac{\alpha_{m+\frac{1}{2},n}I_{m+\frac{1}{2},n} - \alpha_{m-\frac{1}{2},n}I_{m-\frac{1}{2},n}}{\omega_{m,n}} = \dfrac{r\sigma}{\epsilon}\left(\dfrac{1}{2\pi}\bar{\phi} - I_{m,n}\right), \\ I_{m,n}(z_i, r, t)|_{t=t^k} = I_{m,n,0}(z_i, r, t^k), \end{cases} \tag{3.10}$$

where the function $\bar{\phi}$ and the initial value $I_{m,n,0}$ will be reconstructed later. For Eq. (3.10), a formal time-dependent evolution solution can be obtained,

$$\begin{aligned} & r_{j-1/2}I_{m,n}(t, z_i, r_{j-1/2}, \mu_{m,n}, \xi_{m,n}) \\ = \ & \mathrm{e}^{-\nu_{i,j-1/2}(t-t^k)}\widehat{rI_{m,n,0}}\left(z_i, r_{j-1/2} - \tfrac{c\mu_{m,n}}{\epsilon}(t-t^k), t^k\right) \\ & + \int_{t^k}^{t} \mathrm{e}^{-\nu_{i,j-1/2}(t-s)}\frac{c\sigma_{i,j-1/2}}{2\pi\epsilon^2}\widehat{r\bar{\phi}}\left(z_i, r_{j-1/2} - \frac{c\mu_{m,n}}{\epsilon}(t-s), s\right)\mathrm{d}s \\ & - \int_{t^k}^{t} \mathrm{e}^{-\nu_{i,j-1/2}(t-s)}\frac{c\left(\alpha_{m+\frac{1}{2},n}\hat{I}_{i,j-1/2,m+\frac{1}{2},n} - \alpha_{m-\frac{1}{2},n}\hat{I}_{i,j-1/2,m-\frac{1}{2},n}\right)}{\epsilon\,\omega_{m,n}}\mathrm{d}s, \end{aligned} \tag{3.11}$$

where $\nu = c\sigma/\epsilon^2$ and $\nu_{i-1/2,j}$ denotes the value of ν at the cell interface. The function $\widehat{rI_{m,n,0}}(z_i, r, t^k)$ is the reconstruction of $rI_{m,n,0}(z_i, r, t^k)$ which will be given later, and $\widehat{r\bar{\phi}}$ is defined similarly. Substituting the formula (3.11) into Eq. (3.9) and integrating in time from t^k to t^{k+1}, we can get the numerical flux $H_{i,j-1/2,m,n}$ in the r-direction. The numerical flux $H_{i,j+1/2,m,n}$ can be obtained in the same manner.

The cell boundary values $\hat{I}_{i,j-1/2,m+\frac{1}{2},n}, \hat{I}_{i,j-1/2,m-\frac{1}{2},n}$ in (3.11) can be obtained through the upwind approach,

$$\hat{I}_{i,j-1/2,m+\frac{1}{2},n} = \begin{cases} I^k_{i,j-1,m+\frac{1}{2},n}, & \text{if } \mu_{m,n} > 0, \\ I^k_{i,j,m+\frac{1}{2},n}, & \text{if } \mu_{m,n} < 0. \end{cases}$$

Similarly, we get

$$\hat{I}_{i,j-1/2,m-\frac{1}{2},n} = \begin{cases} I^k_{i,j-1,m-\frac{1}{2},n}, & \text{if } \mu_{m,n} > 0, \\ I^k_{i,j,m-\frac{1}{2},n}, & \text{if } \mu_{m,n} < 0. \end{cases}$$

The initial function $\widehat{rI_{m,n,0}}$ in (3.11) is constructed by a piecewise linear reconstruction:

$$\widehat{rI_{m,n,0}}(z_i, r, t^k) = \begin{cases} r_{i,j-1} I^k_{i,j-1,m,n} + \delta_r (rI)^k_{i,j-1,m,n}(r - r_{i,j-1}), & \text{if } r < r_{j-1/2}, \\ r_{i,j} I^k_{i,j,m,n} + \delta_r (rI)^k_{i,j,m,n}(r - r_{i,j}), & \text{if } r > r_{j-1/2}. \end{cases} \tag{3.12}$$

Here $\delta_r (rI)^k_{i,j-1,m,n} = r_{i,j-1}\delta_r I^k_{i,j-1,m,n} + I^k_{i,j-1,m,n}$ and $\delta_r (rI)^k_{i,j,m,n} = r_{i,j}\delta_r I^k_{i,j,m,n} + I^k_{i,j,m,n}$, where $\delta_r I^k_{i,j-1,m,n}, \delta_r I^k_{i,j,m,n}$ are the reconstructed slopes at cell center $(i, j-1)$ and (i, j) in the r-direction, respectively, where the second-order MUSCL-type slope limiter [24] is used to remove spurious oscillations.

The function $\widehat{r\tilde{\phi}}(z_i, r, t)$ is implicitly constructed by

$$\begin{aligned} \widehat{r\tilde{\phi}}(z_i, r, t) \; &= r_{j-1/2}\left(\phi^{k+1}_{i,j-1/2} + \delta_t \phi^{k+1}_{i,j-1/2}(t - t^{n+1})\right) \\ &+ \begin{cases} \delta_r (r\phi)^{k+1,L}_{i,j-1/2}(r - r_{j-1/2}), & \text{if } r < r_{j-1/2}, \\ \delta_r (r\phi)^{k+1,R}_{i,j-1/2}(r - r_{j-1/2}), & \text{if } r > r_{j-1/2}, \end{cases} \end{aligned} \tag{3.13}$$

where

$$\delta_r (r\phi)^{k+1,L}_{i,j-1/2} = r_{j-1/2}\delta_r \phi^{k+1,L}_{i,j-1/2} + \phi^{k+1}_{i,j-1}$$

and

$$\delta_r (r\phi)^{k+1,R}_{i,j-1/2} = r_{j-1/2}\delta_r \phi^{k+1,R}_{i,j-1/2} + \phi^{k+1}_{i,j}.$$

The unknown cell boundary value $\phi^{k+1}_{i,j-1/2}$ and the slopes $\delta_r \phi^{k+1,L}_{i,j-1/2}, \delta_r \phi^{k+1,R}_{i,j-1/2}, \delta_t \phi^{k+1}_{i,j-1/2}$ will be determined in the next subsection.

3.4 Macroscale Evolution Equations

The unified gas kinetic scheme updates both microscopic and macroscopic variables [19, 20]. The function $\tilde{\phi}$ in (3.9) and the unknowns in (3.13) can be determined by solving the following macroscopic equations, which are obtained by taking angular moment of the first equation in (2.1). With the definition $\rho = \int I \mathrm{d}\vec{\Omega}$, and keeping in mind that $\phi = acT^4$, we take the angle integration of $(2.1)_1$ to obtain the following macroscopic system:

$$\begin{cases} \dfrac{\epsilon}{c}\dfrac{\partial \rho}{\partial t} + \nabla \cdot \left\langle \vec{\Omega} I \right\rangle = \dfrac{\sigma}{\epsilon}(\phi - \rho), \\ \epsilon^2 C_v \dfrac{\partial T}{\partial t} \equiv \epsilon^2 \dfrac{\partial U}{\partial t} = \sigma(\rho - \phi), \end{cases} \tag{3.14}$$

where we have denoted the angular vector integration $\left\langle \vec{\Omega} I \right\rangle$ by

$$\left\langle \vec{\Omega} I \right\rangle = \int \vec{\Omega} I \mathrm{d}\vec{\Omega} = \int (\xi, \mu) I \mathrm{d}\xi \mathrm{d}\omega,$$

and the gradient operator ∇ is in *RZ*-cylindrical coordinates. For a function f, the divergence operator reads as

$$\nabla \cdot f = \frac{1}{r}\frac{\partial rf}{\partial r} + \frac{\partial f}{\partial z}.$$

To obtain the macro-quantities ρ and ϕ at the next time step through Eq. (3.14), we first define an exact relationship between the material energy density U and the radiation energy density ϕ by

$$\beta(x,t) = \frac{\partial \phi}{\partial U} = \frac{\mathrm{d}\phi}{\mathrm{d}T}\frac{\mathrm{d}T}{\mathrm{d}U} = \frac{4acT^3}{C_v(T)}. \tag{3.15}$$

Then, the system (3.14) can be rewritten as

$$\begin{cases} \dfrac{\epsilon}{c}\dfrac{\partial \rho}{\partial t} + \nabla \cdot \left\langle \vec{\Omega} I \right\rangle = \dfrac{\sigma}{\epsilon}(\phi - \rho), \\ \epsilon^2 \dfrac{\partial \phi}{\partial t} = \beta\sigma(\rho - \phi). \end{cases} \tag{3.16}$$

Thus, the finite volume discretization of the system (3.16) can be written as

$$\begin{cases} \rho_{i,j}^{k+1} = \rho_{i,j}^{k} + \frac{\Delta t}{V_{i,j}}\left(\Phi_{i-1/2,j}^{k+1} - \Phi_{i+1/2,j}^{k+1}\right) \\ + \frac{\Delta t}{V_{i,j}}\left(\Psi_{i,j-1/2}^{k+1} - \Psi_{i,j+1/2}^{k+1}\right) + \frac{\sigma_{i,j}^{k+1} c \Delta t}{\epsilon^2}\left(\phi_{i,j}^{k+1} - \rho_{i,j}^{k+1}\right), \\ \phi_{i,j}^{k+1} = \phi_{i,j}^{k} + \frac{(\beta\sigma)_{i,j}^{k+1}\Delta t}{\epsilon^2}\left(\rho_{i,j}^{k+1} - \phi_{i,j}^{k+1}\right), \end{cases} \tag{3.17}$$

where the above macro-cell interface fluxes are given through micro-fluxes from (3.9) as follows:

$$\begin{aligned} \Phi_{i-1/2,j}^{k+1} &= \sum_{n=1}^{N}\sum_{m=1}^{M_n} F_{i-\frac{1}{2},j,m,n}\omega_{m,n}, \\ \Phi_{i+1/2,j}^{k+1} &= \sum_{n=1}^{N}\sum_{m=1}^{M_n} F_{i+\frac{1}{2},j,m,n}\omega_{m,n}, \\ \Psi_{i,j-1/2}^{k+1} &= \sum_{n=1}^{N}\sum_{m=1}^{M_n} H_{i,j-\frac{1}{2},m,n}\omega_{m,n}, \\ \Psi_{i,j+1/2}^{k+1} &= \sum_{n=1}^{N}\sum_{m=1}^{M_n} H_{i,j+\frac{1}{2},m,n}\omega_{m,n}. \end{aligned} \tag{3.18}$$

Thus, based on the macro-interface fluxes, Eq. (3.17) reduce to a coupled nonlinear system of the macro-quantities $\phi_{i,j}^{k+1}$ and $\rho_{i,j}^{k+1}$ only, where the parameters $\sigma_{i,j}^{k+1}$ and $\beta_{i,j}^{k+1}$ depend implicitly on the material temperature $T_{i,j}^{k+1}$. This nonlinear system can be solved by an iterative method [19, 20].

After obtaining $\phi_{i,j}^{k+1}$ iteratively, we take $\tilde{\phi}$ in (3.9) as

$$\tilde{\phi} = \phi_{i,j}^{k+1}, \quad \text{and} \quad \phi_{i,j-1/2}^{k+1} = \left(\phi_{i,j}^{k+1} + \phi_{i,j-1}^{k+1}\right)/2$$

is the cell boundary value in (3.13). The left and right one-sided finite differences in (3.13) are given by

$$\delta_r \phi_{i,j-1/2}^{k+1,L} = \frac{\phi_{i,j-1/2}^{k+1} - \phi_{i,j-1}^{k+1}}{\Delta r/2}, \quad \delta_r \phi_{i,j-1/2}^{k+1,R} = \frac{\phi_{i,j}^{k+1} - \phi_{i,j-1/2}^{k+1}}{\Delta r/2}.$$

For the time derivative $\delta_t \phi_{i,j-1/2}^{k+1}$ in (3.13), we use

$$\delta_t \phi_{i,j-1/2}^{k+1} = \frac{\phi_{i,j-1/2}^{k+1} - \phi_{i,j-1/2}^{k}}{\Delta t}.$$

At this point, with the determined macroscopic variables in Eq. (3.17), the radiation intensity in Eq. (3.8) can be updated, which is the main procedure in our unified gas kinetic scheme. Then, the final step is to solve the second equation in (2.1) to give the material temperature with the newly obtained value $I_{i,j,m,n}^{k+1}$. The solution for the energy equation $(3.17)_2$ is given by

$$\hat{\phi}_{i,j}^{k+1} = \frac{\phi_{i,j}^{k} + \Delta t(\beta\sigma)_{i,j}^{k+1} \sum_{n=1}^{N} \sum_{m=1}^{M_n} \omega_{m,n} I_{i,j,m,n}^{k+1}/\epsilon^2}{1 + \Delta t(\beta\sigma)_{i,j}^{k+1}/\epsilon^2}. \tag{3.19}$$

Based on (3.19), the material temperature is determined by $T_{i,j}^{k+1} = (\hat{\phi}_{i,j}^{k+1}/(ac))^{1/4}$. This completes the construction of our UGKS scheme for the gray radiative transfer equations (2.1).

3.5 Summary of the Algorithm

In this subsection, we summarize the above solution procedure to the following algorithm for convenience.

Loop of UGKS: Given $I_{i,j,m,n}^{k}$ and $T_{i,j}^{k}$, one has $\rho_{i,j}^{k}$ and $\phi_{i,j}^{k}$. Find $I_{i,j,m,n}^{k+1}$ and $T_{i,j}^{k+1}$.

(i) With $I_{i,j,m,n}^{k}$ in hand, use (3.18) to calculate the macro-flux. Solve the system (3.17) to obtain $\phi_{i,j}^{k+1}$, $\rho_{i,j}^{k+1}$.

(ii) With the obtained values $\phi_{i,j}^{k+1}$ and $\rho_{i,j}^{k+1}$ from the step (i), solve the resulting equation (3.8) for $I_{i,j,m,n}^{k+1}$.

(iii) With the solution $I_{i,j,m,n}^{k+1}$, solve (3.19) to get $\hat{\phi}_{i,j}^{k+1}$, and then the new material temperature $T_{i,j}^{k+1}$.

(iv) Go to the next computational step.

End

Now, the algorithm loop of our asymptotic preserving scheme for the gray radiative transfer equations in cylindrical coordinates is complete. In the next section, we give the asymptotic analysis of the above-constructed numerical scheme.

4 Asymptotic Analysis of UGKS

In this section, we adapt the idea in [17] to show that the above UGKS is asymptotic preserving (AP). The numerical flux plays a dominant role for the AP property. Firstly, the numerical flux in the r-direction

$$H_{i,j-1/2,m,n} = \frac{c\mu_{m,n}\Delta z}{\epsilon\Delta t}\int_{t^k}^{t^{k+1}} r_{i,j-1/2} I_{m,n}(t, z_i, r_{j-1/2}, \mu_{m,n}, \xi_{m,n})\mathrm{d}t$$

can be exactly computed [19, 20]. From Eq. (3.11), we have

$$\begin{aligned} H_{i,j-1/2,m,n} &= \Delta z\Big\{ A_{i,j-1/2}\mu_{m,n}\Big((rI)^{k,-}_{i,j-1/2,m,n}1_{\mu_{m,n}>0} + (rI)^{k,+}_{i,j-1/2,m,n}1_{\mu_{m,n}<0}\Big) \\ &+D_{i,j-1/2}\Big(\mu^2_{m,n}\delta_r(r\phi)^{k+1,L}_{i,j-1/2}1_{\mu_{m,n}>0} + \mu^2_{m,n}\delta_r(r\phi)^{k+1,R}_{i,j-1/2}1_{\mu_{m,n}<0}\Big) \\ &+B_{i,j-1/2}\Big(\mu^2_{m,n}\delta_r(rI)^{k}_{i,j-1,m,n}1_{\mu_{m,n}>0} + \mu^2_{m,n}\delta_r(rI)^{k}_{i,j,m,n}1_{\mu_{m,n}<0}\Big) \\ &+r_{j-1/2}\Big(Q_{i,j-1/2}\mu_{m,n}\delta_t\phi^{k+1}_{i,j-1/2} + C_{i,j-1/2}\mu_{m,n}\phi^{k+1}_{i,j-1/2}\Big) \\ &+P_{i,j-1/2}\mu_{m,n}\Big(\frac{\alpha_{m+1/2,n}I^{k+1}_{i,j-1,m+1/2,n} - \alpha_{m-1/2,n}I^{k+1}_{i,j-1,m-1/2,n}}{\omega_{m,n}}1_{\mu_{m,n}>0} \\ &+\frac{\alpha_{m+1/2,n}I^{k+1}_{i,j,m+1/2,n} - \alpha_{m-1/2,n}I^{k+1}_{i,j,m-1/2,n}}{\omega_{m,n}}1_{\mu_{m,n}<0}\Big)\Big\}, \end{aligned} \tag{4.1}$$

where $(rI)^{k,-}_{i,j-1/2,m,n}, (rI)^{k,+}_{i,j-1/2,m,n}$ are used to denote the interface values with

$$\begin{aligned} (rI)^{k,-}_{i,j-1/2,m,n} &= r_{i,j-1}I^k_{i,j-1,m,n} + \delta_r(rI)^k_{i,j-1,m,n}(r_{j-1/2} - r_{i,j-1}), \\ (rI)^{k,+}_{i,j-1/2,m,n} &= r_{i,j}I^k_{i,j,m,n} + \delta_r(rI)^k_{i,j,m,n}(r_{j-1/2} - r_{i,j}). \end{aligned}$$

The coefficients in (4.1) are given by

$$\begin{aligned} A &= \frac{c}{\epsilon\Delta t\nu}\left(1 - \mathrm{e}^{-\nu\Delta t}\right), \\ C &= \frac{c^2\sigma}{2\pi\Delta t\epsilon^3\nu}\left(\Delta t - \frac{1}{\nu}\left(1 - \mathrm{e}^{-\nu\Delta t}\right)\right), \\ D &= -\frac{c^3\sigma}{2\pi\Delta t\epsilon^4\nu^2}\left(\Delta t(1 + \mathrm{e}^{-\nu\Delta t}) - \frac{2}{\nu}\left(1 - \mathrm{e}^{-\nu\Delta t}\right)\right), \\ B &= -\frac{c^2}{\epsilon^2\nu^2\Delta t}\left(1 - \mathrm{e}^{-\nu\Delta t} - \nu\Delta t\mathrm{e}^{-\nu\Delta t}\right), \\ Q &= \frac{c^2\sigma}{2\pi\epsilon^3\nu^3\Delta t}\left(1 - \mathrm{e}^{-\nu\Delta t} - \nu\Delta t\mathrm{e}^{-\nu\Delta t} - \frac{1}{2}(\nu\Delta t)^2\right), \\ P &= -\frac{c^2}{\Delta t\epsilon^2\nu}\left(\Delta t - \frac{1}{\nu}\left(1 - \mathrm{e}^{-\nu\Delta t}\right)\right) \end{aligned} \tag{4.2}$$

with $\nu = \frac{c\sigma}{\epsilon^2}$. With the expression (4.2), we have

$$\begin{aligned}
A_{i,j-1/2} &= A(\Delta t, \epsilon, \sigma_{i,j-1/2}, \nu_{i,j-1/2}),\\
C_{i,j-1/2} &= C(\Delta t, \epsilon, \sigma_{i,j-1/2}, \nu_{i,j-1/2}),\\
D_{i,j-1/2} &= D(\Delta t, \epsilon, \sigma_{i,j-1/2}, \nu_{i,j-1/2}),\\
B_{i,j-1/2} &= B(\Delta t, \epsilon, \sigma_{i,j-1/2}, \nu_{i,j-1/2}),\\
Q_{i,j-1/2} &= Q(\Delta t, \epsilon, \sigma_{i,j-1/2}, \nu_{i,j-1/2}),\\
P_{i,j-1/2} &= P(\Delta t, \epsilon, \sigma_{i,j-1/2}, \nu_{i,j-1/2}).
\end{aligned} \tag{4.3}$$

On the other hand, for the z-direction, the interface flux $F_{i-\frac{1}{2},j}$ is given by

$$F_{i-1/2,j,m,n} = \frac{cS_{i-1/2,j}\xi_{m,n}}{\epsilon\Delta t}\int_{t^k}^{t^{k+1}} I_{m,n}(t, z_{i-1/2}, r_j, \mu_{m,n}, \xi_{m,n})\mathrm{d}t,$$

which can be expressed by

$$\begin{aligned}
F_{i-1/2,j,m,n} &= S_{i-1/2,j}\Big\{A_{i-1/2,j}\xi_{m,n}\Big(I^{k,-}_{i-1/2,j,m,n}1_{\xi_{m,n}>0} + I^{k,+}_{i-1/2,j,m,n}1_{\xi_{m,n}<0}\Big)\\
&\quad + D_{i-1/2,j}\Big(\xi^2_{m,n}\delta_z\phi^{k+1,L}_{i-1/2,j}1_{\xi_{m,n}>0} + \xi^2_{m,n}\delta_z\phi^{k+1,R}_{i-1/2,j}1_{\xi_{m,n}<0}\Big)\\
&\quad + B_{i-1/2,j}\Big(\xi^2_{m,n}\delta_z I^k_{i-1,j,m,n}1_{\xi_{m,n}>0} + \xi^2_{m,n}\delta_z I^k_{i,j,m,n}1_{\xi_{m,n}<0}\Big)\\
&\quad + Q_{i-1/2,j}\xi_{m,n}\delta_t\phi^{k+1}_{i-1/2,j} + C_{i-1/2,j}\xi_{m,n}\phi^{k+1}_{i-1/2,j}\Big\}.
\end{aligned} \tag{4.4}$$

Here $I^{k,-}_{i-1/2,j,m,n}, I^{k,+}_{i-1/2,j,m,n}$ are interface values given by

$$\begin{aligned}
I^{k,-}_{i-1/2,j,m,n} &= I^k_{i-1,j,m,n} + \delta_z I^k_{i-1,j,m,n}(z_{i-1/2} - z_{i-1,j}),\\
I^{k,+}_{i-1/2,j,m,n} &= I^k_{i,j,m,n} + \delta_z I^k_{i,j,m,n}(z_{i-1/2} - z_{i,j}),
\end{aligned}$$

where $\delta_z I^k_{i-1,j,m,n}$ and $\delta_z I^k_{i,j,m,n}$ are slopes in the z-direction and can be constructed similar to those in the r-direction above.

The behavior of the scheme in the small ϵ limit is completely determined by the property of the coefficient functions that are given by

Proposition 1 *Let σ be positive. Then, as ϵ tends to zero, we have*

- $A(\Delta t, \epsilon, \sigma, \nu)$ *tends to 0*;
- $B(\Delta t, \epsilon, \sigma, \nu)$ *tends to 0*;
- $D(\Delta t, \epsilon, \sigma, \nu)$ *tends to* $-c/(2\pi\sigma)$;
- $P(\Delta t, \epsilon, \sigma, \nu)$ *tends to* $-c/\sigma$.

In the following, we use the notation $\int_{2\pi}\mathrm{d}\mu\mathrm{d}\xi$ to denote the angular integration in the half sphere. Thus, the corresponding macroscopic diffusion flux $\Phi^{k+1}_{i-1/2,j}$ in the z-direction, defined by

$$\begin{aligned}
\Phi^{k+1}_{i-1/2,j} &= \Big\langle \tfrac{cS_{i-1/2,j}\xi}{\epsilon\Delta t}\int_{t^k}^{t^{k+1}} I(t, z_{i-1/2}, r_j, \mu, \xi)\mathrm{d}t\Big\rangle\\
&= \int_{2\pi}\tfrac{cS_{i-1/2,j}\xi}{\epsilon\Delta t}\int_{t^k}^{t^{k+1}} I(t, z_{i-1/2}, r_j, \mu, \xi)\mathrm{d}t\mathrm{d}\mu\mathrm{d}\xi
\end{aligned} \tag{4.5}$$

has the following limit:

$$\begin{aligned}\Phi^{k+1}_{i-1/2,j} &= S_{i-1/2,j}\sum_{n=1}^{N}\sum_{m=1}^{M_n}\omega_{m,n}F_{i-1/2,j,m,n}\\ &\xrightarrow[\epsilon\to 0]{} -S_{i-1/2,j}\left(\frac{c}{6\sigma_{i-1/2,j}}\delta_z\phi^{k+1,L}_{i-1/2,j}+\frac{c}{6\sigma_{i-1/2,j}}\delta_z\phi^{k+1,R}_{i-1/2,j}\right)\\ &= -\frac{cS_{i-1/2,j}}{3\sigma_{i-1/2,j}}\frac{\phi^{k+1}_{i,j}-\phi^{k+1}_{i-1,j}}{\Delta z}.\end{aligned} \tag{4.6}$$

The limit (4.6) gives a numerical flux of the asymptotic limiting equation (2.2) in the z-direction.

On the other hand, the corresponding macroscopic diffusion flux $\Psi^{k+1}_{i,j-1/2}$ in the r-direction, defined by

$$\begin{aligned}\Psi^{k+1}_{i,j-1/2} &= \left\langle\frac{c\mu\Delta z}{\epsilon\Delta t}\int_{t^k}^{t^{k+1}} r_{j-1/2}I(t,z_i,r_{j-1/2},\mu,\xi)\mathrm{d}t\right\rangle\\ &= \int_{2\pi}\frac{c\mu\Delta z}{\epsilon\Delta t}\int_{t^k}^{t^{k+1}} r_{j-1/2}I(t,z_i,r_{j-1/2},\mu,\xi)\mathrm{d}t\mathrm{d}\mu\mathrm{d}\xi\end{aligned} \tag{4.7}$$

has the following limit:

$$\begin{aligned}\Phi^{k+1}_{i,j-1/2} &= \Delta z\sum_{n=1}^{N}\sum_{m=1}^{M_n}\omega_{m,n}H_{i,j-1/2,m,n}\\ &\xrightarrow[\epsilon\to 0]{} -S_{i,j-1/2}\left(\frac{c}{6\sigma_{i,j-1/2}}\delta_r\phi^{k+1,L}_{i,j-1/2}+\frac{c}{6\sigma_{i,j-1/2}}\delta_r\phi^{k+1,R}_{i,j-1/2}\right)\\ &\quad-\frac{c\Delta z}{\sigma_{i,j-1/2}}\sum_{n=1}^{N}\sum_{m=1}^{M_n}\omega_{m,n}\mu_{m,n}\\ &\quad\times\left\{\left(\mu_{m,n}\frac{\phi^{k+1}_{i,j}}{2\pi}+\frac{\alpha_{m+1/2,n}I^{k+1}_{i,j,m+1/2,n}-\alpha_{m-1/2,n}I^{k+1}_{i,j,m-1/2,n}}{\omega_{m,n}}\right)1_{\mu_{m,n}<0}\right.\\ &\quad\left.+\left(\mu_{m,n}\frac{\phi^{k+1}_{i,j-1}}{2\pi}+\frac{\alpha_{m+1/2,n}I^{k+1}_{i,j-1,m+1/2,n}-\alpha_{m-1/2,n}I^{k+1}_{i,j-1,m-1/2,n}}{\omega_{m,n}}\right)1_{\mu_{m,n}>0}\right\}\\ &= -\frac{cS_{i,j-1/2}}{3\sigma_{i,j-1/2}}\frac{\phi^{k+1}_{i,j}-\phi^{k+1}_{i,j-1}}{\Delta r}-\frac{c\Delta z}{\sigma_{i,j-1/2}}\sum_{n=1}^{N}\sum_{m=1}^{M_n}\omega_{m,n}\mu_{m,n}\\ &\quad\times\left\{\left(\mu_{m,n}\frac{\phi^{k+1}_{i,j}}{2\pi}+\frac{\alpha_{m+1/2,n}I^{k+1}_{i,j,m+1/2,n}-\alpha_{m-1/2,n}I^{k+1}_{i,j,m-1/2,n}}{\omega_{m,n}}\right)1_{\mu_{m,n}<0}\right.\\ &\quad\left.+\left(\mu_{m,n}\frac{\phi^{k+1}_{i,j-1}}{2\pi}+\frac{\alpha_{m+1/2,n}I^{k+1}_{i,j-1,m+1/2,n}-\alpha_{m-1/2,n}I^{k+1}_{i,j-1,m-1/2,n}}{\omega_{m,n}}\right)1_{\mu_{m,n}>0}\right\}.\end{aligned} \tag{4.8}$$

The limit (4.8) gives a numerical flux of the limiting equation (2.2) in the r-direction.

Next, we shall see that the above constructed UGKS for the radiative transfer equations (2.1) is in fact asymptotic preserving, which is verified in the following proposition.

Proposition 2 *Let σ be positive. Then, as ϵ tends to zero, the numerical scheme given by* (3.8) *and* (3.9) *approaches to the standard implicit diffusion scheme for the diffusion limit equation* (2.2) *in cylindrical coordinates.*

Proof Firstly, in view of the order ϵ^{-2} term in the non-starting direction equation (3.8), as the parameter ϵ tends to zero, one has

$$I^{k+1}_{i,j,m,n} \to \frac{1}{2\pi}\phi^{k+1}_{i,j}. \tag{4.9}$$

Integrating the above equation with respect to the angular variable, we obtain as $\epsilon \to 0$ that

$$\rho^{k+1}_{i,j} \to \phi^{k+1}_{i,j} = ac\left(T^{k+1}_{i,j}\right)^4. \tag{4.10}$$

Similarly, for the starting direction equation (3.2), in view of the order ϵ^{-2} term in its discretization equation, as the parameter ϵ tends to zero, we get

$$I^{k+1}_{i,j,1/2,n} \to \frac{1}{2\pi}\phi^{k+1}_{i,j}. \tag{4.11}$$

Secondly, for the order ϵ^{-1} term in Eq. (3.8), such as the left flux $F^{k+1}_{i-1/2,j,m,n}$ given by the formula (4.4), integrating the flux $F^{k+1}_{i-1/2,j}$ in the angular variable, we obtain the macro-flux $\Phi^{k+1}_{i-1/2,j,m,n}$ in Eq. (4.6). As $\epsilon \to 0$, we deduce by Proposition 1 that

$$\Phi^{k+1}_{i-1/2,j} \to -\frac{cS_{i-1/2,j}}{3\sigma^{k+1}_{i-1/2,j}}\frac{\phi^{k+1}_{i,j} - \phi^{k+1}_{i-1,j}}{\Delta z}. \tag{4.12}$$

Similarly, as $\epsilon \to 0$, the right macro-interface flux implies

$$\Phi^{k+1}_{i+1/2,j} \to -\frac{cS_{i+1/2,j}}{3\sigma^{k+1}_{i+1/2,j}}\frac{\phi^{k+1}_{i,j} - \phi^{k+1}_{i+1,j}}{\Delta z}. \tag{4.13}$$

For the lower r-direction boundary flux $H^{k+1}_{i,j-1/2,m,n}$ given by Eq. (4.1), integrating the flux $H^{n+1}_{i,j-1/2,m,n}$ in the angular variable, we have the macro-flux $\Psi^{k+1}_{i,j-1/2}$ in Eq. (4.8). By the relations in (3.1), (3.3), (4.9), (4.11), and Proposition 1, as $\epsilon \to 0$ we infer that

$$\Psi^{k+1}_{i,j-1/2} \to -\frac{cS_{i,j-1/2}}{3\sigma^{k+1}_{i,j-1/2}}\frac{\phi^{k+1}_{i,j} - \phi^{k+1}_{i,j-1}}{\Delta r}. \tag{4.14}$$

Similarly, as $\epsilon \to 0$, the right macro-interface flux goes to

$$\Psi^{n+1}_{i,j+1/2} \to -\frac{cS_{i,j+1/2}}{3\sigma^{k+1}_{i,j+1/2}}\frac{\phi^{k+1}_{i,j} - \phi^{k+1}_{i,j+1}}{\Delta r}. \tag{4.15}$$

Then, the remaining ϵ^{-1} term in (3.8) satisfies

$$\begin{aligned}&\sum_{n=1}^{N}\sum_{m=1}^{M_n}\omega_{m,n}c\Delta t\frac{\frac{\alpha_{m+1/2,n}}{\tau_{m,n}}I^{k+1}_{i,j,m,n} - \left(\frac{1-\tau_{m,n}}{\tau_{m,n}}\alpha_{m+1/2,n} + \alpha_{m-1/2,n}\right)I^{k+1}_{i,j,m-1/2,n}}{V_{i,j}\omega_{m,n}/A_{i,j}}\\ &= \frac{c\Delta t A_{i,j}}{V_{i,j}}\sum_{n=1}^{N}\sum_{m=1}^{M_n}\left(\alpha_{m+1/2,n}I^{k+1}_{i,j,m+1/2,n} - \alpha_{m-1/2,n}I^{k+1}_{i,j,m-1/2,n}\right) = 0.\end{aligned} \tag{4.16}$$

Thirdly, adding Eq. (3.8) to (3.19), integrating the resulting equation in the angular variable, and using (4.12), (4.13), (4.14), (4.15) and (4.16), we see that

$$\begin{aligned}\rho_{i,j}^{k+1} &= \rho_{i,j}^{k} + \frac{\Delta t}{V_{i,j}}\left(-\frac{cS_{i-1/2,j}}{3\sigma_{i-1/2,j}^{k+1}}\frac{\phi_{i,j}^{k+1}-\phi_{i-1,j}^{k+1}}{\Delta z} + \frac{cS_{i+1/2,j}}{3\sigma_{i+1/2,j}^{k+1}}\frac{\phi_{i,j}^{k+1}-\phi_{i+1,j}^{k+1}}{\Delta z}\right)\\ &+ \frac{\Delta t}{V_{i,j}}\left(-\frac{cS_{i,j-1/2}}{3\sigma_{i,j-1/2}^{k+1}}\frac{\phi_{i,j}^{k+1}-\phi_{i,j-1}^{k+1}}{\Delta r} + \frac{cS_{i,j+1/2}}{3\sigma_{i,j+1/2}^{k+1}}\frac{\phi_{i,j}^{k+1}-\phi_{i,j+1}^{k+1}}{\Delta r}\right) - c(\phi_{i,j}^{k+1} - \phi_{i,j}^{k})/\beta_{i,j}^{k+1}.\end{aligned} \tag{4.17}$$

By virtue of the relation (4.10), Eq. (4.17) is a standard five-point scheme for the diffusion equation (2.2) in cylindrical coordinates. Therefore, this shows that our UGKS for the gray radiative transfer equations (2.1) is asymptotic preserving (AP), where the current UGKS can capture the exact diffusion solution without the constraint on the cell size being smaller than the photon's mean free path.

5 Numerical Examples

In this section, we present numerical examples arising from inertial confinement fusion to validate the proposed AP-UGKS in cylindrical coordinates. In the computation, the unit of the length is centimeter, the mass unit is gramme (g), the time unit is nanosecond (ns), the temperature unit is kilo electronvolt (KeV), and the energy unit is 10^9 Joules (GJ). With the above units, the light speed is 29.98 cm/ns and the radiation constant a is 0.013 72 GJ/cm^3 KeV^4. For angle discretization, we take $N = 8$ in the following simulations.

Example 1 (see [1]) The computational domain is given in Fig. 2. It is a thirteen-millimeters square with a thin wall of material around the outside edge. There are two

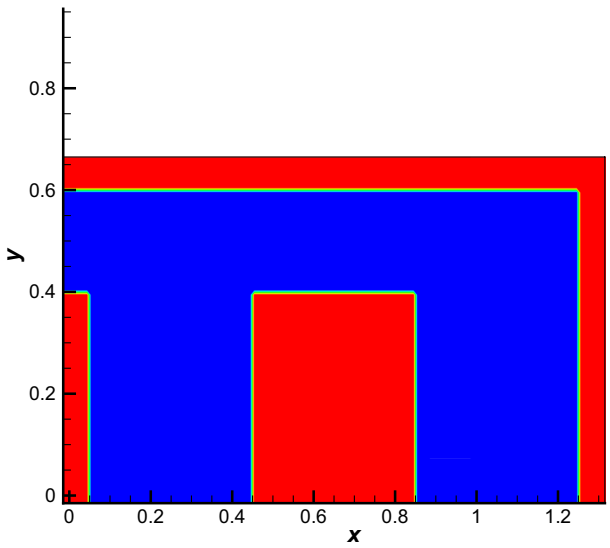

Fig. 2 The computation region for Example 1. The red regions are optically thick region, and the blue region is vacuum region. This is an axial symmetric problem

millimeter openings on the left side of the hohlraum, and there is a rectangular block of material in the center of the system. The material is a purely absorber with $\sigma_a = 100\,\mathrm{cm}^{-1}$ and $\rho C_v = 5.0 \times 10^5\,\mathrm{J/m^3K}$. The rest of the device is a void with zero opacity. The initial material and radiation temperatures are set to be $T_0 = 300\,\mathrm{K}$. A source boundary condition is applied along the entire left hand side. The source has a temperature of $T_{\mathrm{source}} = 3.5 \times 10^6\,\mathrm{K}$. To show the performance of the numerical scheme, we calculated the problem with coarse mesh with 130×65 cells and fine mesh with 260×130 cells, respectively. In Fig. 3, we give the contours of both material and radiative temperatures at time = 1 ns in the upper half region since the problem is cylindrically symmetric. And in Figs. 4 and 5 we compare the results of two mesh cases at line $y = 0.05$ and $y = 0.39$, respectively. Further in Fig. 6, we compare the time evolution values of material and radiation temperatures at two points (0.005, 0.005) and (0.46, 0.39) in both mesh cases. It is clear to see that the current UGKS can simulate the vacuum region and the optical thick region accurately.

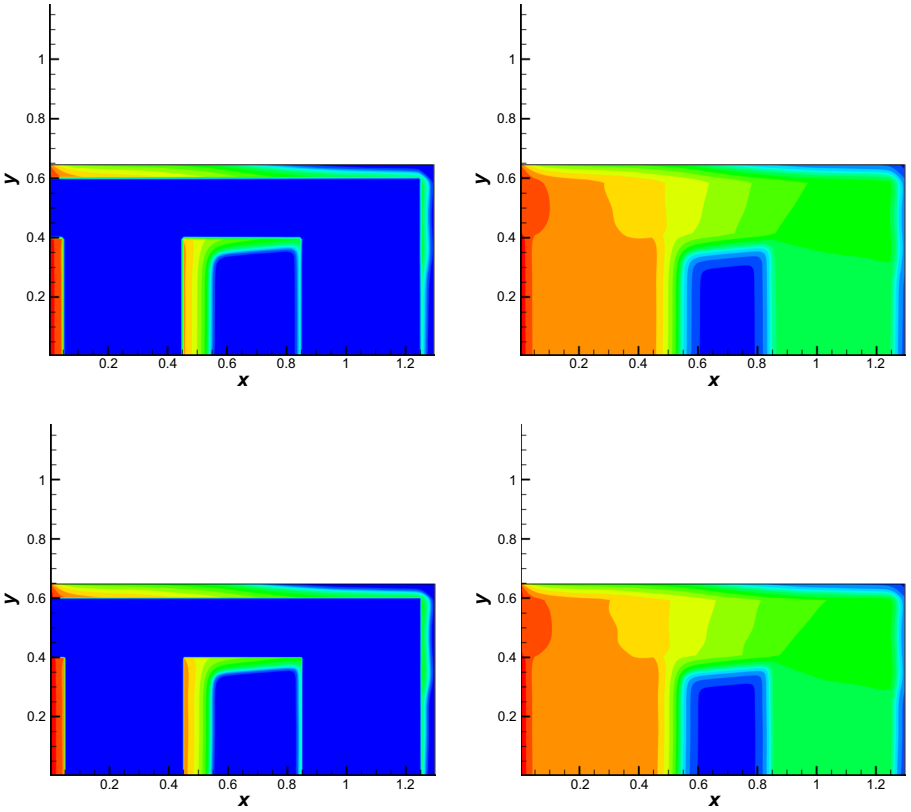

Fig. 3 The contours of material and radiation temperature for Example 1 at time = 1 ns. The left sub-figures are the material temperatures, and the right sub-figures are the radiation temperature. The above two figures are calculated by coarse mesh with 130×65 cells, while the bottom two figures are calculated by fine mesh with 260×130 cells

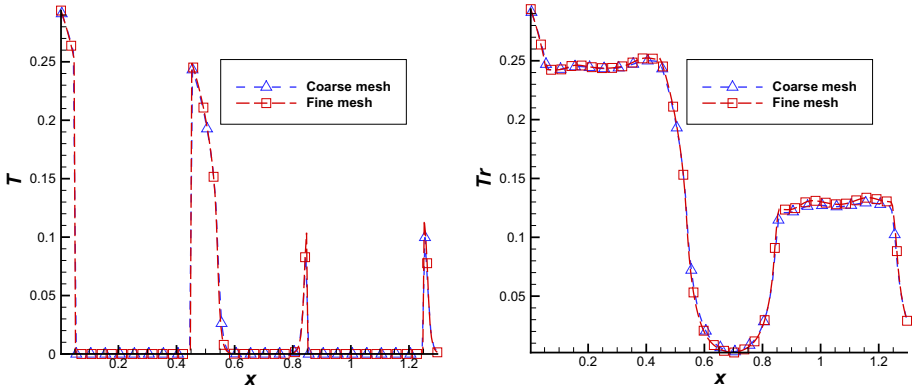

Fig. 4 The comparing results of UGKS for material and radiation temperatures at $y = 0.05$ cm and time = 1 ns with coarse and fine meshes. The left one is the material temperature, and the right one is the radiation temperature

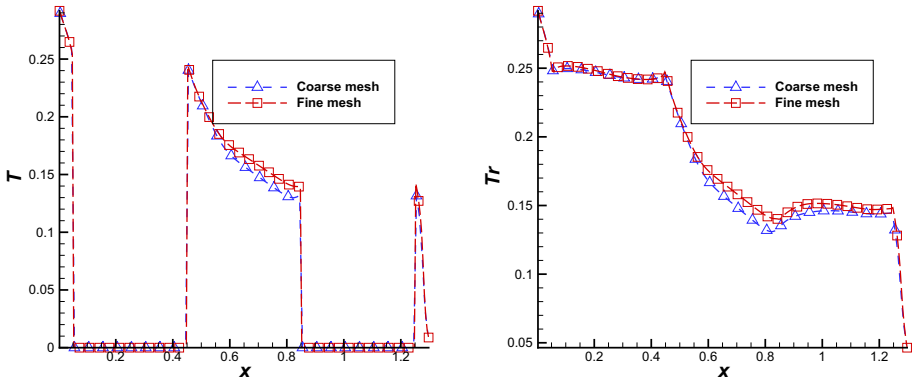

Fig. 5 The comparing results of UGKS for material and radiation temperatures at $y = 0.39$ cm and time = 1 ns with coarse and fine meshes. The left one is the material temperature, and the right one is the radiation temperature

Example 2 (see [16]) In this test we solve a simplified hohlraum problem. The layout is given in Fig. 7, where the red regions have $\sigma = 100T^{-3}\,\mathrm{cm}^{-1}$ for T in KeV and the blue region is vacuum. On the left boundary, there is a 1KeV blackbody source-emitting radiation into the initially cold material. In Fig. 8, we give the contours of material and radiative temperature at time=10 ns. To validate the solutions, we present the computed results by both UGKS and the implicit Monte Carlo (IMC) method (see [3, 4, 14]) for the temperatures in Figs. 9 and 10 along the two lines of $z = 0.05$ and $z = 0.44$, respectively. In Figs. 11 and 12, we show the temperature evolution computed by both UGKS and the IMC method at two points (0.105, 0.005) and (0.56, 0.44), respectively. It is obvious to see that both UGKS and the IMC method can simulate the transport in vacuum and optical thick regions, while UGKS gives a smooth transition in different transport regimes. The comparison of computation time for UGKS and IMC is given in Table 1; here, the computation platform is LENOVO personal computer with Intel(R) Core(TM) i7-4770 CPU, and with

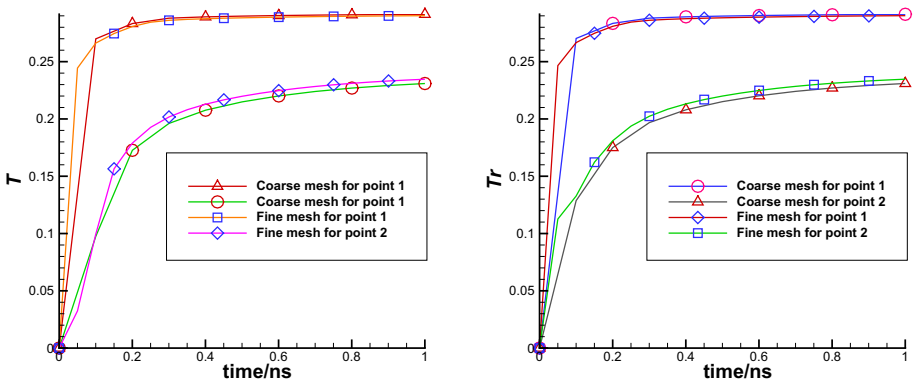

Fig. 6 The comparing coarse and fine mesh results of UGKS for material and radiation temperatures at points (0.105, 0.005) and (0.46, 0.39) with time evolution. The left one is the material temperature, and the right one is the radiation temperature

Table 1 The computation time comparison for UGKS and IMC

UGKS (min)	IMC (min)
293	3 405

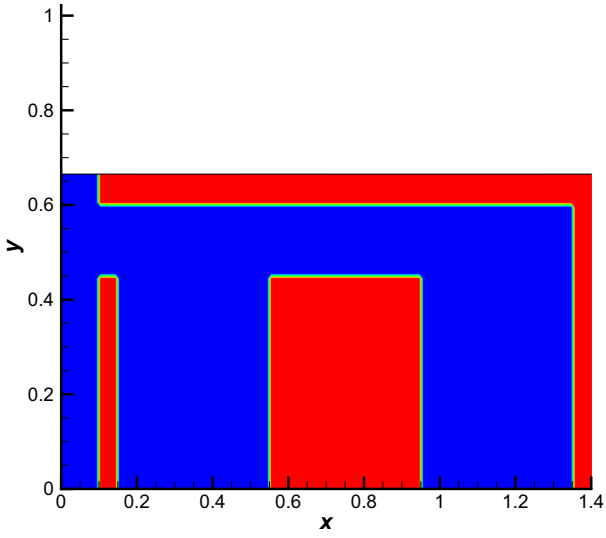

Fig. 7 The computation region for Example 2, the red regions are optically thick region, and the blue region is vacuum region. This is an axial symmetric problem

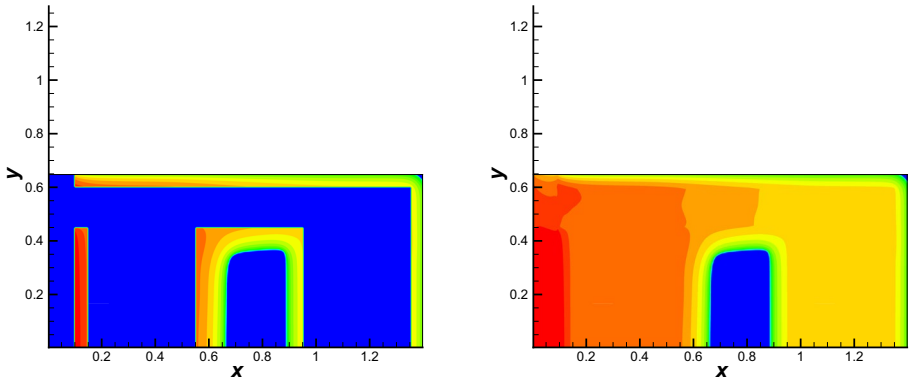

Fig. 8 The contours of material and radiation temperature for Example 2 at time = 10 ns. The left one is the material temperature, and the right one is the radiation temperature

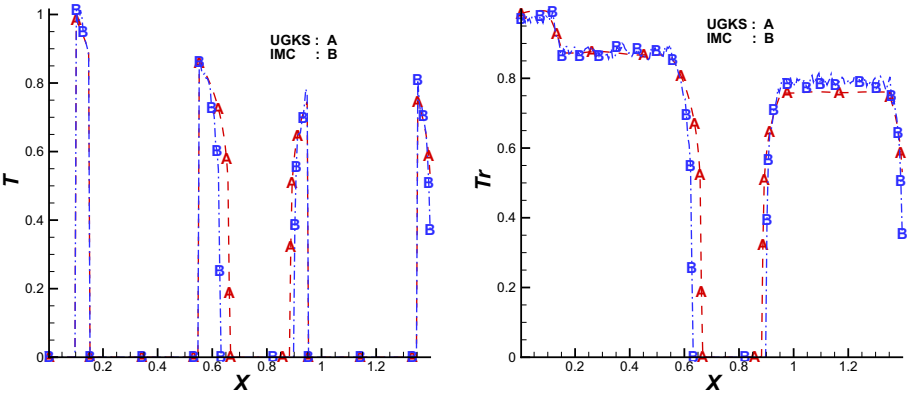

Fig. 9 The results of UGKS and IMC for material and radiation temperatures at $y = 0.05$ cm and time = 10 ns. The left one is the material temperature, and the right one is the radiation temperature

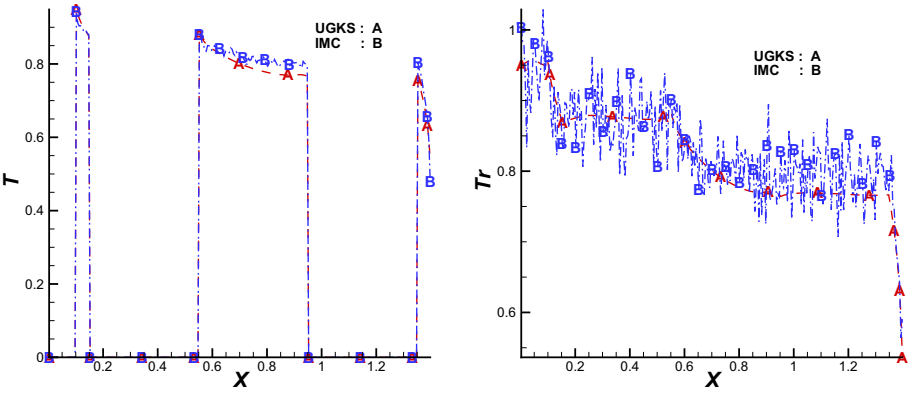

Fig. 10 The results of UGKS and IMC for material and radiation temperatures at $y = 0.44$ cm and time = 10 ns. The left one is the material temperature, and the right one is the radiation temperature

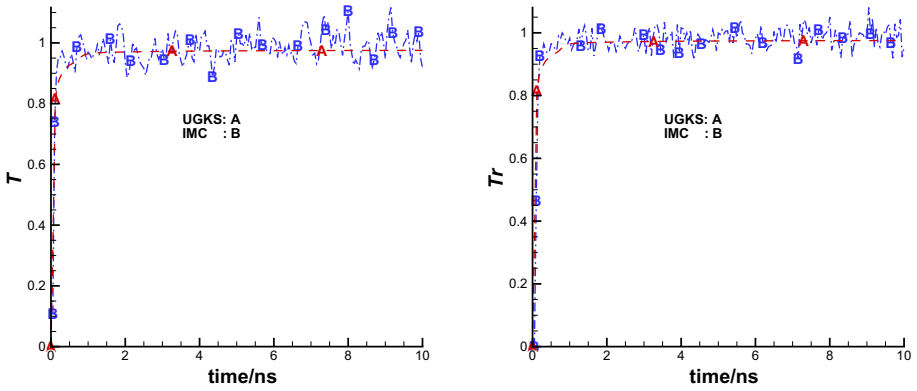

Fig. 11 The results of UGKS and IMC for material and radiation temperatures at point (0.105, 0.005) with time evolution. The left one is the material temperature, and the right one is the radiation temperature

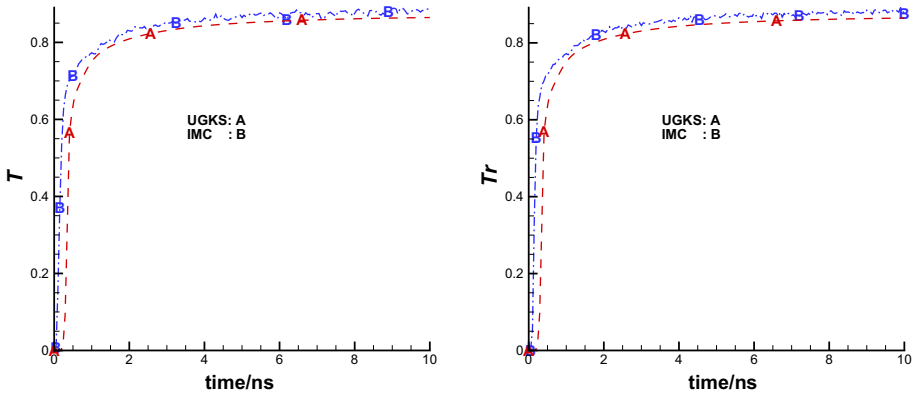

Fig. 12 The results of UGKS and IMC for material and radiation temperatures at point (0.56, 0.44) with time evolution. The left one is the material temperature, and the right one is the radiation temperature

1 million particles in IMC simulation. From this, we can see that the UGKS can save the computational time greatly.

6 Conclusion

In this paper, we present a unified gas kinetic scheme (UGKS) for the gray radiative transfer equations in cylindrical geometry. Due to the time-dependent un-splitting treatment of photon transport and collision in the flux evaluation, the current UGKS can give accurate solutions in all transport regimes. It has asymptotic preserving property in the optical thick region to recover the diffusion solution without using a mesh size being smaller than the photon mean free path. At the same time, accurate solutions can be obtained by UGKS in the optical thin regime, even the free transport solution in vacuum

regime. For a physical problem with multiscale transport in different regions, the current UGKS gives a smooth transition from the optically thin to optically thick regions with the variation of the ratio between the time step and local photon's collision time. The cylindrical hohlram examples in inertial confinement fusion are tested to validate the current approach. The current scheme can be naturally extended to the study of coupled system among radiative transfer [20], fluid dynamics [25], and plasma physics [15].

Acknowledgements The authors wish to thank all referees for their useful suggestions to improve the current paper. The research of Sun is supported by NSFC (Grant nos. 11671048, 91630310) and CAEP Project (2015B0202041, 2015B0202040); Jiang is supported by the National Basic Research Program under Grant 2014CB745002 and NSFC (Grant no. 11631008); and Xu is supported by Hong Kong research Grant council (16206617,16207715) and NSFC (Grant nos. 11772281,91530319).

References

1. Brunner, T.A.: Forms of Approximate Radiation Transport. Technical Report SAND2002-1778, Sandia National Laboratories (2002)
2. Chen, S.Z., Xu, K., Lee, C.B., Cai, Q.D.: A unified gas kinetic scheme with moving mesh and velocity space adaptation. J. Comput. Phys. **231**, 6643–6664 (2012)
3. Fleck JR, J.A., Cummings, J.D.: An implicit Monte Carlo scheme for calculating time and frequency dependent nonlinear radiation transport. J. Comput. Phys. **8**, 313–342 (1971)
4. Gentile, N.A.: Implicit Monte Carlo diffusion—an accerlation method for Monte Carlo time-dependent radiative transfer simulations. J. Comput. Phys. **172**, 543–571 (2001)
5. Huang, J.C., Xu, K., Yu, P.B.: A unified gas-kinetic scheme for continuum and rarefied flows II: multi-dimensional cases. Commun. Comput. Phys. **12**, 662–690 (2012)
6. Jin, S., Levermore, C.D.: The discrete-ordinate method in diffusive regimes. Transp. Theory Stat. Phys. **20**, 413–439 (1991)
7. Jin, S., Levermore, C.D.: Fully discrete numerical transfer in diffusive regimes. Transp. Theory Stat. Phys. **22**, 739–791 (1993)
8. Jin, S., Pareschi, L., Toscani, G.: Uniformly accurate diffusive relaxation schemes for multiscale transport equations. SIAM J. Numer. Anal. **38**, 913–936 (2000)
9. Klar, A.: An asymptotic-induced scheme for nonstationary transport equations in the diffusive limit. SIAM J. Numer. Anal. **35**, 1073–1094 (1998)
10. Larsen, A.W., Morel, J.E.: Asymptotic solutions of numerical transport problems in optically thick, diffusive regimes. II. J. Comput. Phys. **83**, 212–236 (1989)
11. Larsen, E.W., Pomraning, G.C., Badham, V.C.: Asymptotic analysis of radiative transfer problems. J. Quant. Spectrosc. Radiat. Transf. **29**, 285–310 (1983)
12. Larsen, A.W., Morel, J.E., Miller Jr., W.F.: Asymptotic solutions of numerical transport problems in optically thick, diffusiive regimes. J. Comput. Phys. **69**, 283–324 (1987)
13. Lee, C.E.: The Discrete S_N Approximation to Transport Theory, LA-2595 (1962)
14. Li, S., Li, G., Tian, D.F., Deng, L.: An implicit Monte Carlo method for thermal radiation transport. Acta Phys. Sin. **62**, 249501 (2013)
15. Liu, C., Xu, K.: A unified gas kinetic scheme for continuum and rarefied flows V: multiscale and multi-component plasma transport. Commun. Comput. Phys. **22**, 1175–1223 (2017)
16. McClarren, R.G., Hauckb, C.D.: Simulating radiative transfer with filtered spherical harmonics. Phys. Lett. A. **374**, 2290–2296 (2010)
17. Mieussens, L.: On the asymptotic preserving property of the unified gas kinetic scheme for the diffusion limit of linear kinetic model. J. Comput. Phys. **253**, 138–156 (2013)
18. Morel, J.E., Montry, G.R.: Analysis and elimination of the discrete ordinates flux dip. Transp. Theory Stat. Phys. **13**, 615–633 (1984)
19. Sun, W.J., Jiang, S., Xu, K.: An asymptotic preserving unified gas kinetic scheme for gray radiative transfer equations. J. Comput. Phys. **285**, 265–279 (2015)
20. Sun, W.J., Jiang, S., Xu, K., Li, S.: An asymptotic preserving unified gas kinetic scheme for frequency-dependent radiative transfer equations. J. Comput. Phys. **302**, 222–238 (2015)
21. Sun, W.J., Zeng, Q.H., Li, S.G.: The asymptotic preserving unified gas kinetic scheme for gray radiative transfer equations on distorted quadrilateral meshes. Ann. Differ. Eqs. **2**, 141–165 (2016)

22. Sun, W.J., Jiang, S., Xu, K.: An implicit unified gas kinetic scheme for radiative transfer with equilibrium and non-equilibrium diffusive limits. Commun. Comput. Phys. **22**, 899–912 (2017)
23. Sun, W.J., Jiang, S., Xu, K.: A multidimensional unified gas-kinetic scheme for radiative transfer equations on unstructured mesh. J. Comput. Phys. **351**, 455–472 (2017)
24. van Leer, B.: Towards the ultimate conservative difference schemes V. A second-order sequal to Godunov's method. J. Comput. Phys. **32**, 101–136 (1979)
25. Xu, K., Huang, J.C.: A unified gas-kinetic scheme for continuum and rarefied flows. J. Comput. Phys. **229**, 7747–7764 (2010)